FUNDAMENTALS & APPLICATIONS

CHEMELECTROCHEM

ANALYSIS & CATALYSIS, BIO & NANO, ENERGY & MORE

Accepted Article

Title: Self-standing membranes consisting of inherently chiral electroactive oligomers: electrosynthesis, characterization and preliminary tests in potentiometric setups

Authors: Serena Arnaboldi, Daniele Vigo, Mariangela Longhi, Francesco Orsini, Sephira Riva, Sara Grecchi, Elena Giacovelli, Vittoria Guglielmi, Roberto Cirilli, Giovanna Longhi, Giuseppe Mazzeo, Tiziana Benincori, and Patrizia Romana Mussini

To be cited as: *ChemElectroChem* 10.1002/celc.201900779

Link to VoR: http://dx.doi.org/10.1002/celc.201900779

A Journal of

ChemPubSoc Europe

WILEY-VCH

www.chemelectrochem.org

ARTICLE WILEY-VCH

Self-standing membranes consisting of inherently chiral electroactive oligomers: electrosynthesis, characterization and preliminary tests in potentiometric setups

Serena Arnaboldi* [a], Daniele Vigo [a], Mariangela Longhi [a], Francesco Orsini [b], Sephira Riva [a], Sara Grecchi [a], Elena Giacovelli [a], Vittoria Guglielmi [a], Roberto Cirilli [c], Giovanna Longhi [d], Giuseppe Mazzeo [d], Tiziana Benincori [e], Patrizia R. Mussini* [a]

Dedicated to Professor Torquato Mussini on the occasion of his 85th birthday

Abstract: Self-standing chiral electroactive synthetic membranes are presented, prepared by oxidative electrooligomerization of a thiophene-based "inherently chiral" electroactive monomer on indium tin oxide ITO or fluorine doped tin oxide FTO electrodes, followed by detachment of the electrodeposited thin films in aqueous solution. The membranes, possibly mesoporous, consist of a mixture of open and cyclic "inherently chiral" oligomers, *i.e.* in which both chirality and electroactivity originate from the same source, the main conjugated backbone featuring a tailored torsion; such a combination can afford outstanding chirality manifestations. The electrosynthesis conditions significantly modulate the oligomer distribution. Racemate films are compared to enantiopure ones. Circular dichroism confirms that (*R*)- or (*S*)- enantiopure films are obtained starting from the corresponding (*R*)- or (*S*)- enantiopure monomers. Reliable transmembrane potential readings are obtained in preliminary tests in ion-selective electrode (ISE)-like setups, consistent with those predicted considering the membrane features, a first step towards extension of the protocol to chiral experiments.

1. Introduction

Chiral membranes are important tools for enantiomer discrimination or/and separation in a broad range of applications, some of them already mature, particularly concerning preparative separations in the pharmaceutic field [1,2]. Many chiral membranes are of natural origin (*e.g.* polysaccharides, polyaminoacid derivatives), or based on natural chiral components (like proteins, amino acids, nucleic acids, enzymes...) while less common so far are membranes based on synthetic chiral components (*e.g.* calixarenes or crown ethers) [1]. However, synthetic chiral membranes, like more generally synthetic chiral selectors, have interesting intrinsic features, like wide range of molecular designs and functional properties, equal availability of both enantiomers, and easy synthesis scalability.

Among analytical applications of chiral membranes, a potentially interesting one concerns implementation as key components in chiral potentiometric sensors. Actually the so far still limited proposed approaches to chiral potentiometry include chiral ionophores (chiral crown ethers, antibiotics, calixarenes, chiral complex anions or cations, alkaloids...) as key components of "liquid membranes" or graphite-based pastes, implemented in ISE-like set ups [3-6]; electrode modification with molecularly imprinted polymer films MIPs prepared with chiral templates [7]; electrode modification with chiral electroactive oligomer films [8]. Furthermore, conducting oligo- or polymer films, enabling charge carrier transduction on account of their combining ion transport and electron transfer, look excellent materials for all-solid-state ISEs (developed since the early 70's but dramatically improved in the last two decades with availability of conducting polymers) [9,10]. A necessary condition for developing chiral potentiometric sensors is that the chiral probe should be either a charged species, or if neutral in itself, either ionizable (*e.g.* through an acid-base equilibrium) [8,11,12], or converted in a salt through alkylation (*e.g.* of suitable nitrogen positions) or functionalization with a convenient charged substituent [13]; as an alternative, a MIP-based sensor can first capture a neutral chiral probe and then exchange it with a charged mimic species [14,15].

Concerning design of synthetic membranes, different stereogenic elements can be considered to endow them with chirality, the most common ones being localized stereocentres. However, it was recently observed for different kinds of chiral selectors, including chiral electroactive oligomer films, that much better enantioselection performances can be obtained by implementation of the "inherent chirality" strategy [16,17]. In "inherently chiral" polyconjugated molecular materials both chirality and key functional properties originate from the same structural element, which can coincide with the whole main molecular scaffold, featuring a tailored torsion with an energy barrier too high to be

[a] Dr S. Arnaboldi, Mr D. Vigo, Dr M. Longhi, Dr S. Riva, Ms S. Grecchi, Ms E. Giacovelli, Dr V. Guglielmi, Prof P. R. Mussini
Dipartimento di Chimica
Università degli Studi di Milano
Via Golgi 19, 20133, Milano, Italy
serena.arnaboldi@unimi.it; patrizia.mussini@unimi.it
[b] Dr. F. Orsini
Dipartimento di Fisica "Aldo Pontremoli"
Università degli Studi di Milano
Via Celoria 16, 20133, Milano, Italy
[c] Dr. R. Cirilli
Centro Nazionale per il Controllo e la Valutazione dei Farmaci,
Istituto Superiore di Sanità
Viale Regina Elena 299, 00161 Roma, Italy
[d] Prof G. Longhi, Dr. G. Mazzeo
Dipartimento di Medicina Molecolare e Traslazionale
Università degli Studi di Brescia
Sezione di Fisica c/o, Viale Europa 11, 25123 Brescia, Italy
[e] Prof T. Benincori
Dipartimento di Scienza e Alta tecnologia
Università degli Studi dell'Insubria
Via Valleggio 11, 22100 Como, Italy

Supporting information for this article is given via a link at the end of the document.

overcome at room temperature; regioregularity enables propagating such property into foldamer-/helical-like macro- or supramolecular structures [16,17]. Large potential differences have been observed between enantiomers of various chiral probes in voltammetry experiments implementing inherent chirality at electrode|solution interphases by modifying achiral electrodes with enantiopure inherently chiral electroactive films electrodeposited from different heterocycle-based monomers with atropoisomeric cores (*i.e.* consisting of two moieties with hindered reciprocal rotation) [18-22] or with helical shape (*i.e.* tetrathiahelicene) [23]. Among them, the parent and so far more extensively studied one is 2-[5-(2,5'-bithienyl)]thianaphthene BT_2T_4 (Scheme 1) [18-20] consisting of a bibenzothiophene atropoisomeric core (with approximately 80° torsional angle and 167 kJ mol^{-1} related energy barrier [18]) and two bithiophene wings with homotopic α thiophene terminals available for oligomerization.

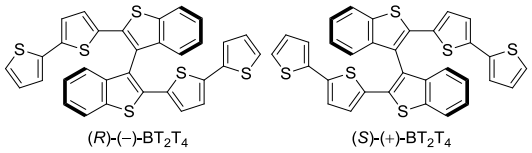

Scheme 1

By electrooligomerization of enantiopure BT_2T_4 monomers the corresponding enantiopure oligomer films can be obtained, consisting of a mixture of open and closed oligomers having the same configuration as the starting monomer, as confirmed by the nicely specular circular dichroism CD spectra of the enantiopure films [18]. The resulting modified electrodes showed impressive enantiodiscrimination performances with different chiral probes in voltammetric experiments. [18-20]

Most interestingly, we are now showing that electrosynthesized oligo-BT_2T_4 films can be peeled off from the electrode surface after their growth, yielding self-standing chiral membranes. Consisting of open and closed oligomers combining inherent chirality with electroactivity, with both features being indissolubly connected with the π-conjugated oligomeric backbone, they can indeed be regarded as an attractive tool for electroanalytical applications. We have thus extensively characterized them by a multitechnique approach and preliminarily tested them for transmembrane potential readings in classical ISE-like set ups.

2. Results and Discussion

Membrane electrosynthesis

(*R*)- or (*S*)- enantiopure inherently chiral membranes are obtained by potentiodynamic electrooligomerization of the corresponding BT_2T_4 monomer, in a range from 0 V to 1.35 V *vs* SCE, on ITO or FTO electrodes, in ACN+$TBAPF_6$ 0.1M as supporting electrolyte, at 0.05 V/s potential scan rate, to form a thin film of suitable thickness, detachable from the electrode support by immersion in water. (Figure 1)

We had formerly shown that electrooligomerization of BT_2T_4 monomer carried out by potential cycling around its first oxidation peak proceeds very regularly for many cycles, yielding inherently

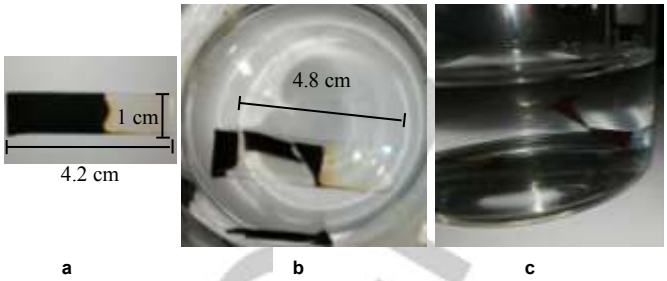

Figure 1. The electrosynthesized membrane on the ITO electrode support (a), while being detached (b) and stored in water (c).

chiral electrode surfaces on different supports in quite different media, including (*i*) dichloromethane (on GC [23,24], on Pt for ESR experiments [18], on Au with EQCM monitoring [24] and on ITO for spectroelectrochemistry [18,25,26]); (*ii*) acetonitrile (on GC for analytical chiral voltammetry experiments [18-20,23], on Pt for *in-situ* conductance measurement [26] and on ITO for electrochemical circular dichroism ones [18,25], and (*iii*) ionic liquid $BMIMPF_6$ (on screen printed electrodes [18,19]).

The electroactive films consisted of an oligomer mixture (from LDI [18]; in particular, open and closed dimers were detected in films deposited on ITO [27]) that could include both open and closed terms, which have been obtained separately by chemical route to be electrochemically and chiroptically characterized [27,28]. Their formation can be explained in terms of the typical thiophene radical cation coupling mechanism [29], with the monomer configuration playing a significant role, too. For example, it has been pointed out that the configuration of (*R,R*)- or (*S,S*)-open dimers promotes cyclization by coupling of the free terminals, unlike the case of (*R,S*)- open dimers, usually resulting in further monomer addition, promoting cyclic trimer formation [28]. The films also exhibited high growth rate and regularity even after many deposition cycles, which can be related to the high three-dimensional character of the starting monomer (on account of the high torsional angle) and to its offering only two homotopic terminals available for the radical cation coupling.

For the electrosynthesis of inherently chiral self supported membranes we have selected as working conditions (*i*) acetonitrile as solvent, granting very high electrodeposition rate [23,30], (*ii*) ITO or FTO as electrode supports for the film growth (*iii*) 50 mV/s electrodeposition rate, resulting in good enantioselection performance for electrodeposited electrode surfaces of the order of several micron thickness [30]; (*iv*) 72 or 108 deposition cycles, to achieve sufficient film thickness to yield a self-standing membrane when detached. In particular, membranes grown with 108 cycles were easier implemented in the ISE setup, even in repeated experiments, while membranes grown with 72 cycles were more convenient for the chiroptical characterization by electronic circular dichroism in transmission mode, requiring a certain degree of membrane transparency. While oligo-BT_2T_4 films are dissolved in $CHCl_3$, we observed that they can be detached in deionized water (Figure 1 (b)), either spontaneously, waiting for a while, or gently promoting their fast detachment by tweezers; self-supported membranes are thus obtained, which can be stored in water (Figure 1 (c)) and managed in the wet

state with the help of a glass pipette. Intriguingly, when transferred from water to ethanol the membranes undergo a sudden color change, from orange/brown to vivid red. Film membrane detachment can be obtained both from ITO and FTO electrode supports.

The detached films were submitted to high resolution LDI analysis, pointing to a mixture of open and closed oligomers, including (spectra synopses and details in SI.1) dimers as prevailing species, as well as trimers, in smaller amounts, and tetramers, in even smaller amounts (in some cases hardly detectable). In particular, by comparison with model LDI spectra for pure cyclic oligomers [27]:

i) in all cases in which 0.1 M $TBAPF_6$ was adopted as supporting electrolyte both open and closed dimers are present in significant amounts. In fact, the approximately estimated closed to open dimer ratio ranges from 2.6-1.6 for films grown on FTO (respectively, from racemate or enantiopure monomer) to 1.13/0.95-0.74 for films grown on ITO (respectively, from racemate, with/without contact with water, or enantiopure monomer), to 0.48 for the film undergoing treatment with isopropanol, resulting in a remarkable color change from orange to vivid red.

ii) in the same cases, the closed to open estimated ratios for trimers are much lower than the corresponding dimer ones at constant conditions; however, again, significantly higher values are obtained on FTO (1.0-0.7 from racemate or enantiopure monomer) respect to ITO (0.11-0.36 from racemate or enantiopure monomer, 0.16 after IprOH treatment).

iii) in the same cases, a quantitative estimation is difficult for the tetramer ratio on account of the low peaks and background noise; however, as for the trimer case, closed ones appear to neatly prevail on open ones.

iv) a peak system is also observed in the m/z range = 1217.8-1223.8, *i.e.* slightly above the dimer one, for which we are considering the possibility of sulphur overoxidation (*e.g.* to sulphoxide), particularly involving the terminal positions in the open dimers.

iv) Incidentally, it is worthwhile noticing that, as expected considering the increasing probability of finding isotopes in a molecule with increasing number of atoms constituting it, the most intense LDI peak in each peak system shifts from the first one for dimers to the third one for trimers, to the fourth one for tetramers.

v) in a special case, in connection with the discussion of FTIR spectra, a (racemate) BT_2T_4 film was electrodeposited from lithium perchlorate ($LiClO_4$) as supporting electrolyte (rather than $TBAPF_6$) in combination with acetonitrile-d3 (CD_3CN) as solvent. Strikingly, in this case the film appeared being practically constituted by closed species, chiefly closed dimers (Fig. SI1.1e). Should the same protocol hold for enantiopure monomers, it might enable to perform enantioselection tests using electrosynthesized films mainly consisting of a single kind of enantiopure oligomer (*i.e.* the closed homochiral dimer, representing a well-defined coordinating cavity).

Starting from (*R*)- or (*S*)-enantiopure BT_2T_4 films, the corresponding (*R*)- or (*S*)-enantiopure membranes are obtained. We confirmed it by electronic circular dichroism ECD, applied to both (*i*) films still attached to the ITO or FTO electrode supports or (*ii*) detached and sandwiched between two quartz slides. (Figure 2)

Reproducibility of the ECD signal while changing the probe orientation and/or side proves that it is genuine ECD without important contributions from linear dichroism and circular birifringence. Care must be taken to avoid distortions due to absorption flattening effects, as reported in reference [31,32]: in our case we could obtain good results with a standard CD setup because of the high quality of films, macroscopically regular and intact also after detachment. Neatly specular (particularly in the FTO case) bisignate signals are obtained for films obtained from BT_2T_4 enantiomers (Figure 2), confirming that chirality and its

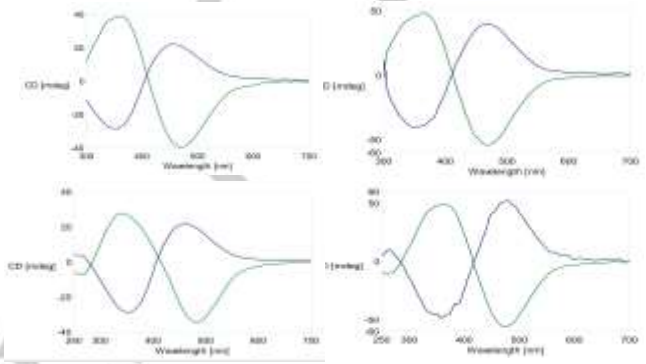

Figure 2 ECD spectra for (*R*)- or (*S*)-enantiopure BT_2T_4 films (green and blue lines, respectively) grown on ITO (left) and FTO (right), both as such (top) and as detached membranes (bottom).

CD sign are fully transferred from monomers to oligomer films; ellipticity maxima are red shifted respect to the monomer ones [18], consistently with the improved conjugation of the oligomers. It can be also noticed that a larger wavelength range is available in the case of the detached membranes, due to the absence of the absorbing oxide support, extension below 250 nm was not possible due to film thickness.

IR spectra

An investigation was carried out for the first time on the FTIR pattern of an electrodeposited oligo-BT_2T_4 film, comparing it to the starting BT_2T_4 monomer as well as to several single BT_2T_4 oligomers (present in the film mixture as confirmed by HR LDI, see former paragraph), available from a previous organic route [27]. A spectra synopsis is reported in Fig. 3 while Table SI2 in the SI summarizes the most important vibrational frequencies for each sample with relevant proposed assignations on the basis of literature data concerning oligothiophene systems [33-37] as well as a former investigation by some of us on the BT_2T_4 monomer [38]. Analogously to the case of the linear α-oligothiophene family [33], all the spectra have a remarkable common pattern, although the BT_2T_4 monomer shows a greater number of bands than all others. Such common pattern includes the signals at ~3060 cm^{-1} (anti-symmetrical stretching of C_β-H [33]), ~1455 cm^{-1} and ~1420 cm^{-1} (symmetrical stretching of C=C in the aromatic rings [35-37]), 1316 cm^{-1} (C_β-C_β stretching [33]), 1157 cm^{-1}, 794-790 cm^{-1} (out-of-plane bending of C_β-H [33,36,37]), 760 cm^{-1} (anti-asymmetrical ring deformation of C-S [34]), ~730 cm^{-1} and 470-480 cm^{-1} (ring deformations [36]), the latter one being notably absent in the film pattern. Characteristic of the BT_2T_4

monomer are the very strong bands at 3104 cm^{-1} (ascribable to the C_α-H symmetrical stretching [33, 34]) and at 840, 822, and 699 cm^{-1} (due to the out-of-plane bending of C_α-H [33-35]) and the band at 547 cm^{-1} (ring deformations [34,37]). A band at ~3100 cm^{-1} can be observed also in the film pattern, although very weak. This is consistent with the film including also open oligomer terms besides closed ones, as confirmed by the above HR LDI analysis. Actually, they are even in significant amount respect to closed ones (about 1:1 for dimers and much more for higher terms). In spite of this, the signal weakness is justified by the C_β-H groups greatly outnumbering the C_α-H ones; even in the smaller open oligomer term, the open dimer, the C_β-H : C_α-H ratio is 16 : 2. Similarly, the C_α-H signal of a linear α-octathiophene, having the same proportion, the C_α-H signal is only slightly perceivable respect to the C_β-H one. [33] Actually the 3200-3000 cm^{-1} range, somehow overlooked in oligothiophene literature respect to the very popular fingerprint region, looks very interesting in our context, since, as we have verified in a preliminary experiment, it could be exploited to investigate the film still attached on the ITO support, while the lower frequency range would be unavailable on account of the support absorption.

Morphological Characterization

The morphology of the three oligomeric membranes, namely oligo-(*S*)-(+)-BT_2T_4, oligo-(*R*)-(–)-BT_2T_4 and racemate oligo-BT_2T_4, was investigated by Scanning Electron Microscopy SEM, Transmission Electron Microscopy TEM, and Tapping Mode Atomic Force Microscopy.

In the case of SEM and AFM the samples were films on the ITO electrode support, without detachment (to ensure the required flatness). In the case of TEM films were electrodeposited on a Ni TEM minigrid in operating conditions similar to those applied for the membrane preparation, but with a small cycle number.

Figure 4 collects SEM images of racemate, (*S*)- and (*R*)- membranes at two increasing magnifications (first and second row).

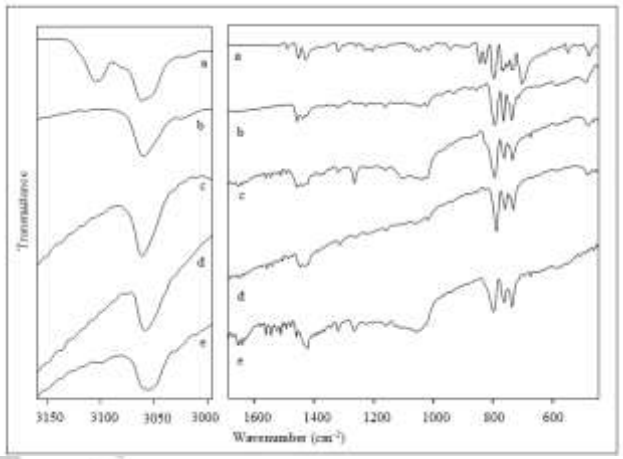

Figure 3 FTIR spectra of (a) BT_2T_4 monomer; (b) a closed BT_2T_4 dimer sample; (c) a closed BT_2T_4 trimer sample; (d) a closed BT_2T_4 tetramer sample; (e) an oligo-BT_2T_4 film electrodeposited on ITO.

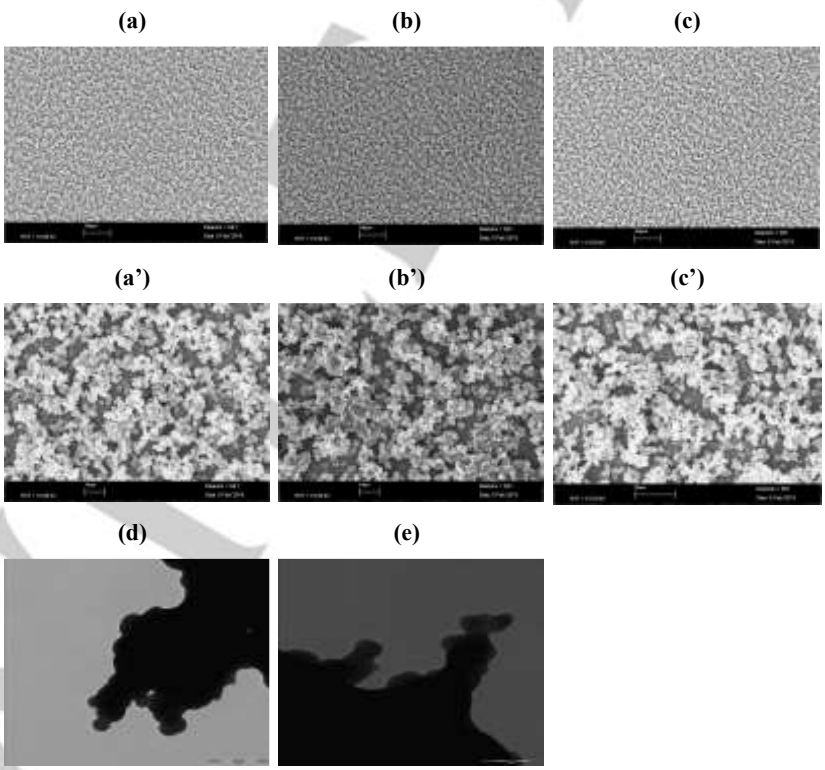

Figure 4. SEM images at 100x (first row) and 750x (second row) magnifications of the three oligomeric membranes: racemate oligo-BT_2T_4 (**a, a'**), oligo-(*S*)-(+)-BT_2T_4 (**b,b'**), and oligo-(*R*)-(–)-BT_2T_4 (**c,c'**).TEM images for racemate oligo-BT_2T_4 (**d**), oligo-(*S*)-(+)-BT_2T_4 (**e**).

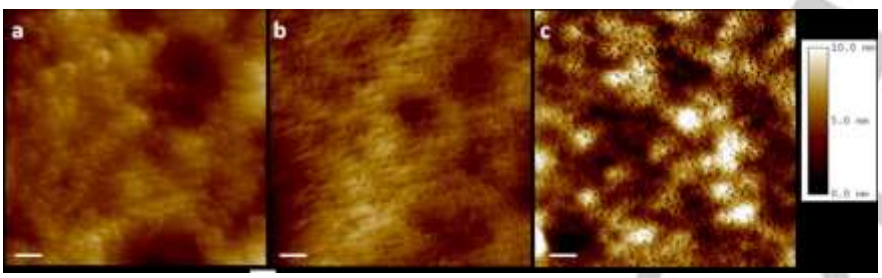

Figure 5. AFM topography images of the three oligomeric membranes: racemate oligo-BT_2T_4 (**a**), oligo-(*S*)-(+)-BT_2T_4 (**b**), oligo-(*R*)-(−)-BT_2T_4 (**c**). For all images: scan area 1x1 μm^2; vertical (color) scale: 10 nm; scale bar: 100 nm.

In the SEM images a uniform globular structure is observed, with particle sizes of the order of hundreds of nanometers; apparently no significant differences can be observed between racemate and enantiopure film at this level.

A similar globular morphology is also well evidenced in the TEM images (Figure 4, third row), although referring to a much thinner film electrodeposited on Ni grid (yet in the same conditions).

As revealed by the SEM images at larger scale (Figure 4, first row), all the membranes, no matter whether enantiopure or racemate, show very similar features: they are constituted by micrometer "patches" deposited inhomogeneously on the whole ITO electrode. This kind of growth, at macroscopic level, gives to the membrane surface a highly porous aspect with relevant differences in height. On the contrary, the single "patches" show a very flat appearance.For this reason, AFM investigation was performed on the single "patches" in order to obtain both information on the membrane morphology at nanometer level and to quantitatively evaluate their surface roughness.

As an example AFM topography images of the three membrane samples are reported in Figure 5.

Considering the SEM/TEM/AFM images at increasing magnification, the surface morphology of the three membranes appears comparable at macroscopic level, but at nanometer scale interesting differences seem to occur. In particular, both (*S*)- and (*R*)- membranes appear to exhibit well-defined structural features of nanometer dimensions, with a central dip (Fig. 5 (b), (c)), unlike the racemate membrane (Fig. 5 (a)), which apparently shows smaller spherical-like structures thus suggesting a different supramolecular organization/arrangement of the single oligomers. The regular dip pattern detected in the enantiopure membrane cases could point to a porous structure, possibly mesoporous according to the dip diameter being of the order of 15 nm; a certain degree of porosity would also be consistent with the specific area, estimated by BET as ~20 cm^2 mg^{-1}.

At nanometer level, the three membranes show a very flat surface. Their RMS surface roughness, obtained analysing several AFM topography images collected in different regions on the membrane, was calculated according the following equation:

$$rms_{xy} = \sqrt{\sum_{x,y=1}^{N} \frac{(Z_{x,y} - Z_{average})^2}{N^2}} \quad (1)$$

where $Z_{average}$ is the average Z value within the examined area, $Z_{x,y}$ is the local Z value, and N indicates the number of points within the area.

The RMS surface roughness values, measured on 500x500 nm^2 areas, for the racemate oligo-BT_2T_4, oligo-(*S*)-(+)-BT_2T_4 and oligo-(*R*)-(−)-BT_2T_4 membranes are reported in Table 1.

Table 1. RMS surface roughness values (on 500x500 nm^2 areas) of the three oligomeric membranes racemate oligo-BT_2T_4, oligo-(*S*)-(+)-BT_2T_4 and oligo-(*R*)-(−)-BT_2T_4, as obtained by AFM imaging.

Sample[l]	RMS surface roughness (nm)
racemate oligo-BT_2T_4	0.62 ± 0.11 (mean ± SD; n = 45)
oligo-(*S*)-(+)-BT_2T_4	1.12 ± 0.23 (mean ± SD; n = 40)
oligo-(*R*)-(−)-BT_2T_4	1.27 ± 0.24 (mean ± SD; n = 50)

Potentiometric membrane tests in classical ISE-like setup

The electrosynthesized membranes were assembled in a ISE-like setup gently placing them on a Teflon® nozzle and filling with the latter the hole in the ISE body cap. (Figure 6a).

They could thus be tested in a potentiometric cell consisting of a sensing membrane electrode and an external reference electrode with in-built salt bridge immersed in a chloride solution, which can be better detailed as in Scheme 2 (with Pt terminals as conventional notation for a regularly open galvanic cell, and with "commercial" polarities, implying the membrane sensing electrode with shielded cable to be connected to the + shielded input of the high-resistance electrometer, no matter what would be the true cell polarity, *i.e.* resulting in a positive reversible potential difference).

The reversible potential difference of the cell can be expressed as

$$E_{cell} = E_{int} - E_{ext} + E_M + E_j \quad (2)$$

where, with reference to Figure 6 (b), E_{ext} is the (constant) potential of the external reference electrode, E_{int} is the (constant) potential of the internal reference electrode, E_M is the membrane potential and E_j is the liquid junction potential, assumed to be minimized by the salt bridge.

$$E_{ext} = E^\circ_{Hg2Cl2|Hg} - k\log a_{Cl\ in\ saturated\ KCl} \quad \text{(constant 1)} \quad (3)$$

$$E_{int} = E^\circ_{AgCl|Ag} - k\log a_{Cl\ in\ CCln\ at\ fixed\ m} \quad \text{(constant 2)} \quad (4)$$

(a)

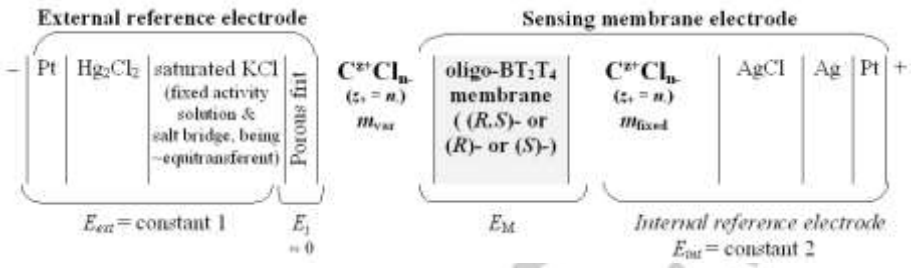

(b)

Figure 6. (a) Assembling an electrosynthesized membrane in the commercial ISE body; (b) detailed galvanic chain of the whole cell assembly.

Thus, the ($E_{int} - E_{ext}$) difference is a constant which can be calculated, although with some approximation as a consequence of the conventional nature of single ion activities. As an alternative, it can be experimentally estimated, by measuring the E_{cell} with identical solutions on the two membrane sides (see further on).
Moreover, $E_j \approx 0$, since the liquid junction potential between external reference electrode and variable solution should be minimized by the saturated KCl salt bridge (especially considering the moderate concentration range of the variable solutions).
Thus we can study the transmembrane potential E_M as

$$E_M \approx E_{cell} - (E_{int} - E_{ext}) \quad (5)$$

To discuss the dependency of the transmembrane potential E_M on the nature and activity of the two adjacent solutions, it is useful to remember that
(*i*) at a non-selective junction between two different solutions in the same solvent, like *e.g.* through a non-selective diaphragm like a porous frit, a potential difference arises, usually termed "liquid junction potential", proportional to the ion activity gradients, and modulated by the differences in cation and anion diffusion coefficients D_i, and implicitly in mobilities u_i (the two quantities being interrelated through the Nernst Einstein equation) in the solvent considered. This can be expressed as

$$dE_{\text{non ion-selective junction}} = \Sigma\tau_j k d\log a_j = \Sigma(t_j/z_j) k d\log a_j \quad (6)$$

in terms of transference numbers in the considered medium, either t_i (classical transference numbers) or τ_j ("signed" transference numbers introduced by Scatchard):

$$t_j = q_j/(\Sigma q_j) = z_j u_j M_j/(\Sigma z_j u_j M_j) \; ; \quad \tau_j = t_j/z_j \quad \Sigma t_j = \Sigma \tau_j z_j = 1 \quad (7)$$

(*ii*) however, ion transference numbers can be modified by specific interactions with "non-innocent" diaphragms; in particular, in the case of an ion-selective membrane, $t_i \rightarrow 1$ for the so called "primary" ion i and $t_j \rightarrow 0$ for the remaining ones; thus equation (5) modifies into

$$dE_{\text{ion-selective junction}} = \tau_i k d\log a_i + \Sigma\tau_j k d\log a_j$$
$$= (t_i/z_i) k d\log a_i + \Sigma(t_j/z_j) k d\log a_j$$
$$\text{with } t_i \rightarrow 1, \text{ all } t_j \rightarrow 0 \; ; \; t_i + \Sigma t_j = \tau_i z_i + \Sigma \tau_j z_j = 1 \quad (8)$$

Thus, for an *ideal* ion-selective membrane

$$dE_{\text{ion-selective junction}} \approx (t_i/z_i) k d\log a_i \rightarrow k/z_i d\log a_i \quad (9)$$

Actually the potential response of an ion-selective electrode is based on the pseudo-Nernstian relationship (9), integrated between the "primary" ion activity in the internal and external solution, and with the addition of the constant potential of the internal reference electrode, expressed as follows (with "commercial" polarity convention) :

$$E_{ISE} \approx E_{\text{int ref}} + k/z_i \log(a_{i,\text{var}}''/a_{i,\text{fixed}}')$$
$$\approx E_{\text{int ref}} + k/z_i \log(a_{i,\text{var}}''/a_{i,\text{fixed}}') \approx U + k/z_i \log(a_{i,\text{var}})$$
(or $U + Q\log(a_{i,\text{var}})$ with a non-ideal membrane) (10)

Different approaches can be adopted to develop an ion-selective membrane [39-41]; in any case, a fundamental issue concerns preventing the counter ion ingress in the membrane concurrently with the primary one to preserve the necessary electroneutrality condition. For our present discussion it is useful to consider the popular, well known case of the so called "liquid" ion-selective membranes, in which an inert polymer like PVC supports a hydrophobic, very viscous solvent/plastifier in which a ionophore is dissolved, selective to the desired primary ion i. Particularly when such ionophore is neutral, it is necessary to add a fourth component in the "membrane cocktail", *i.e.* an electrolyte additive ("ion exchanger") in which the ion with the same sign as primary ion i must have high affinity for the external solvent phase while the ion with opposite sign must have high affinity for the membrane phase. Thus electroneutrality is maintained by exchange of same sign ions rather than concurrent ingress of cation and anion. Now, the present chiral membranes include most of the functionalities of the above described ISE components, namely (i) the support (oligomeric rather than polymeric), (ii) the selector (through the heteroatoms and aromatic systems, particularly cyclic ones) and (iii) the ion-to-electron transducer (when implemented in solid-ISE setups). On the other hand, in the present form it lacks the ion exchanger functionality, although we are developing a starting monomer modified with fixed charge groups. Moreover, the membrane appears mesoporous (as above discussed), with pore sizes of the order of tens of nanometers, which could be modified by changes in the deposition protocol.

For these reasons, we discuss the transmembrane potentials starting from an assumption of non-selective junctions between solutions of a single binary electrolyte $C^{z+}{}_{n+}A^{z-}{}_{n-}$; thus equation (5) becomes

$$dE = (t_C/z_C) k d\log a_C + (t_A/z_A) k d\log a_A$$
$$= (t_C/z_C) k d\log a_C - (t_A/|z_A|) k d\log a_A \quad (11)$$

with $a_C = m_C\gamma_C$ (or $c_C y_C$) $a_A = m_A\gamma_A$ (or $c_A y_A$)
According to the Debye-Hückel convention concerning single ion coefficients:

$$\gamma_C = \gamma_{\pm CA}{}^{zC/|zA|} \quad \gamma_A = \gamma_{\pm CA}{}^{|zA|/zC} \quad (12)$$

Moreover,

$$m_C = n_C m_{CA} \text{ and } m_A = n_A m_{CA} \quad (13)$$

and

$$a_{CA} = n_C{}^{nC} n_A{}^{nA} (m_{CA}\gamma_{\pm CA})^{(nC+nA)} \quad (14)$$

Therefore

$$dE = (t_C/z_C)k\text{dlog}\, n_C m_{CA}\gamma_{\pm CA}^{zC/|zA|} - (t_A/|z_A|)k\text{dlog}\, n_A m_{CA}\gamma_{\pm CA}^{|zA|/zC}$$
$$= (t_C/z_C)k\text{dlog}\, n_C + (t_C/z_C)k\text{dlog}\, m_{CA} + (t_C/|z_A|)k\text{dlog}\, \gamma_{\pm CA}$$
$$-(t_A/|z_A|)k\text{dlog}\, n_A - (t_A/|z_A|)k\text{dlog}\, m_{CA} - (t_A/z_C)k\text{dlog}\, \gamma_{\pm CA}$$
$$= (t_C/z_C - (t_A/|z_A|))k\text{dlog}\, m_{CA} + (t_C/|z_A| - t_A/z_C)k\text{dlog}\, \gamma_{\pm CA} \quad (15)$$

yielding for a 1:1 electrolyte like HCl or KCl:

$$dE = (t_C - t_A)k\text{dlog}\, m_{CA} + (t_C - t_A)k\text{dlog}\, \gamma_{\pm CA}$$
$$= (t_C - t_A)k\text{dlog}\, m_{CA}\gamma_{\pm CA} = (t_C - t_A)k\text{dlog}\, a_{CA}^{1/2}$$
$$= (t_C - t_A)k\text{dlog}\, a_{C=A} \quad (16)$$

and for a 2:1 electrolyte like $CaCl_2$:

$$dE = (t_C/2 - t_A)k\text{dlog}m_{CA} + (t_C - t_A/2)k\text{dlog}\, \gamma_{\pm CA}$$
$$= (t_C/2 - t_A)k\text{dlog}m_C + (t_C - t_A/2)k/2\text{dlog}\, \gamma_C$$
$$\text{or } (t_C/2 - t_A)k\text{dlog}m_A + (t_C - t_A/2)2k\text{dlog}\, \gamma_A \quad (17)$$

Since

$$t_i = z_i u_i M_i / \Sigma z_i u_i M_i \quad (18)$$

and for a binary electrolyte

$$t_+ = n_+\lambda_+/(n_+\lambda_+ + n_-\lambda_-) \quad t_- = n_-\lambda_-/(n_+\lambda_+ + n_-\lambda_-) \quad (19)$$

with λ = ion molar conductances, approximating λ values with tabulated $\lambda°$ ones, we get

for KCl:

$$dE \approx (t_C - t_A)k\text{dlog}\, a_{C=A} \approx -0.0017\text{dlog}\, a_{C=A} \quad (20)$$

for HCl:

$$dE \approx (t_C - t_A)k\text{dlog}\, a_{C=A} \approx 0.037\text{dlog}\, a_{C=A} \quad (21)$$

for $CaCl_2$:

$$dE \approx (t_C/2 - t_A)k\text{dlog}m_C + (t_C - t_A/2)k/2\text{dlog}\, \gamma_C$$
$$\approx -0.0207\text{dlog}\, m_C + 0.0044\text{dlog}\, \gamma_C \quad (22)$$

The experimental membrane potential data observed for the galvanic cell in Figure 6 (b) with a racemate membrane and KCl, or HCl, or $CaCl_2$ as the binary electrolyte at fixed concentration in the internal ISE solution and at variable concentration in the external solution are reported in Table 2 and plotted as a function of loga_{C+} in Figure 7. They show excellent consistency with our predicted values of both E_m *vs* logm_C slopes and of (E_{int} – E_{ext}) biases, confirming that reliable potentials readings can be made across the new membranes in electrochemical setups, as well as confirming our assumption that the membranes in their present state (mesoporosity, absence of fixed negative charges) must behave as non-selective junctions, particularly towards the small ions of the electrolytes chosen as models.

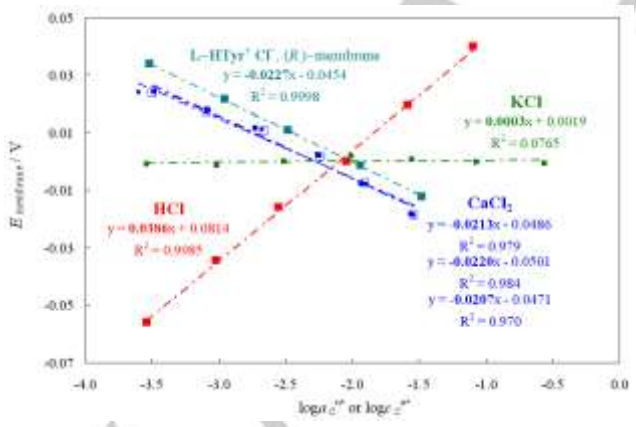

Figure 7. Transmembrane potential readings with our chiral membranes implemented in ISE-like setups with different chloride solutions, as a logarythmic function of the cation activity in the external variable solution.

A preliminary test is also included (Table 2 last row, Figure 7), carried out with L-tyrosine hydrochloride, *i.e.* a chloride probe featuring a larger, chiral cation suitable for chiral experiments. The transmembrane potential readings, plotted in this case *vs* the logarythm of the cation concentration as an acceptable approximation for the cation activity, show, again, a good linear trend, as well as a -0.0226 slope, implying t_{HTyr+} = 0.308 and t_{Cl-} = 0.692, in consistency with the significant bulkiness difference between the two ions.

3. Conclusions

Self-standing electroactive membranes endowed with "inherent chirality", a property implying powerful chirality manifestations, can be easily and conveniently prepared by oxidative electro-oligomerization of a thiophene-based "inherently chiral" electro-active monomer on ITO or FTO electrodes, followed by detachment of the electrodeposited thin films in aqueous solution. The membranes appear to consist of a mixture of open and cyclic inherently chiral oligomers, their distribution being modulated by the experimental conditions (with one case pointing to the attractive possibility of electrosynthesizing a membrane chiefly consisting of closed dimers). Moreover, (*R*)- or (*S*)- enantiopure films can be obtained starting from the corresponding enantiopure monomers.

Among possible applications to be explored, it can be noticed that the new membranes include most of the functionalities of classical ISE components, namely (i) the support (oligomeric rather than polymeric), (ii) the (chiral) selector (through the heteroatoms and aromatic systems, particularly cyclic ones) and (iii) the ion-to-electron transducer (when implemented in solid-ISE setups). Actually reliable transmembrane potential readings are obtained in preliminary tests in ISE-like setups, in excellent consistency with those predicted considering the present membrane features.

Such verification of the protocol soundness is an important first step towards its extension to a systematic program of chiral potentiometric tests performed on all combinations of chiral membrane configurations and of chiral ion concentrations and configurations on each membrane side. Although our membranes are not ionoselective in their present form for the above discussed reasons, the slopes of their linear *E vs* log*a* characteristics reliably account for the mobility difference between cation and anion in the electrolyte solutions on the membrane sides. Such a difference might be modulated not only by the ion nature, as in these first tests, but also, operating with enantiopure membranes and enantiopure ions, by different combinations of membrane and ion configurations.

We are also looking forward to modulating porosity and/or adding an in-built ion exchanger functionality (thus possibly endowing the membrane with ion-selectivity properties), as well as to comparing the membrane performance in classical ISE setups with solid-state ISE ones.

Table 2. Potentiometric tests of transmembrane potential readings in the setup shown in Figure 6 (b) with different chloride electrolytes at constant m_{fixed} and different m_{var} : overall cell potential differences $E_{rev,\ cell}$; estimated and experimental values of potential difference between internal and external reference electrodes ($E_{int} - E_{ext}$); membrane potentials $E_{membrane}$ estimated subtracting ($E_{int} - E_{ext}$) from $E_{rev,\ cell}$; estimated and experimental values of $E_{membrane}$ *vs* $\log a_{C+}$ slopes.

	m_{var} / (mol kg^{-1})	$\gamma_{\pm}$	$\log a_{C+,\ var}$	$E_{rev,\ cell}$ /V	$E_{membrane}$ /V	
KCl *racemic membrane, 108 cycles*	0.000295	0.980	-3.54	0.0978	-0.0008	$E_{membrane}$ *vs* $\log a_{K+}$ slope -0.0017 V (est.) 0.0003±0.0004 V (exp.)
	0.000992	0.965	-3.02	0.0972	-0.0014	
	0.00327	0.939	-2.51	0.0987	0.0001	
	0.0109	0.897	-2.01	0.1004	0.0018	
	0.0331	0.841	-1.56	0.0994	0.0008	
	0.112	0.760	-1.07	0.0984	-0.0002	($E_{int} - E_{ext}$) 0.099 V (est.) 0.097 V (exp.)
	0.411	0.663	-0.56	0.0980	-0.0006	
	m_{fixed} 0.00986	0.902	-2.05			
HCl *racemic membrane, 108 cycles*	0.000295	0.981	-3.54			$E_{membrane}$ vs $\log a_{H+}$ slope -0.037 V (est.) 0.0386±0.0007 V (exp.)
	0.000983	0.966	-3.02	0.0381	-0.0559	
	0.00298	0.943	-2.55	0.0596	-0.0344	
	0.00996	0.905	-2.05	0.0780	-0.016	
	0.0301	0.857	-1.59	0.0940	0	($E_{int} - E_{est}$) 0.099 V (est.) 0.094 V (exp.)
	0.100	0.797	-1.10	0.1136	0.0196	
	m_{fixed} 0.00990	0.966	-2.05	0.134	0.04	
$CaCl_2$ *racemic membrane, 72 cycles*	0.000364	0.929	-3.50	0.1094	0.0239	$E_{membrane}$ *vs* $\log a_{Ca2+}$ slope [-0.0207 V est. neglecting activity coefficient] -0.0213±0.0016V (exp.)
	0.00102	0.887	-3.09	0.1027	0.0172	
	0.00330	0.818	-2.66	0.0962	0.0107	
	0.0110	0.720	-2.24	0.0872	0.0017	
	0.0327	0.617	-1.90	0.0779	-0.0076	($E_{int} - E_{ext}$) 0.083 V (est.) 0.087 V (exp.)
	0.110	0.509	-1.54	0.0669	-0.0186	
	m_{fixed} 0.00991	0.730	-2.28			
$CaCl_2$ *racemic membrane, 108 cycles*	0.000286	0.936	-3.60	0.1103	0.0240	$E_{membrane}$ *vs* $\log a_{Ca2+}$ slope [-0.0207 V est. neglecting activity coefficient] -0.0207±0.0047V (exp.)
	0.00107	0.885	-3.08	0.1039	0.0176	
	0.00312	0.822	-2.68	0.0975	0.0112	
	0.0110	0.720	-2.24	0.0882	0.0019	
	0.0334	0.615	-1.90	0.0784	-0.0079	($E_{int} - E_{ext}$) 0.083 V (est.) 0.088 V (exp.)
	0.111	0509	-1.54	0.0677	-0.0186	
	m_{fixed} 0.0099	0.730	-2.28			
$CaCl_2$ *racemic membrane, 108 cycles*	0.000378	0.928	-3.49	0.1106	0.0244	$E_{membrane}$ *vs* $\log a_{Ca2+}$ slope [-0.0207 V est. neglecting activity coefficient] -0.0220±0.001V (exp.)
	0.00104	0.886	-3.09	0.1039	0.0180	
	0.00270	0.832	-2.73	0.0975	0.0116	
	0.0104	0.725	-2.26	0.0882	0.0023	($E_{int} - E_{ext}$) 0.083 V (est.) 0.088 V (exp.)
	0.0296	0.627	-1.93	0.0784	-0.0075	
	0.103	0.514	-1.56	0.0677	-0.0182	
	m_{fixed} 0.0099	0.730	-2.28			
L-tyrosine hydrochloride *(R)-membrane, 108 cycles*	0.000302					$E_{membrane}$ *vs* $\log m_{HTyr+}$ slope -0.0226±0.0002 V (exp.) →est. transference numbers **t_{HTyr+} = 0.308 t_{Cl-} = 0.692** ($E_{int} - E_{est}$) 0.101 V (exp.)
	0.00110		-3.52	0.1348	0.0341	
	0.00327		-2.96	0.1225	0.0218	
	0.0115		-2.49	0.1117	0.0110	
	0.0332		-1.94	0.0995	-0.0012	
	m_{fixed} 0.00988		-1.48	0.0885	-0.0122	

4. Experimental Section

Preparation and separation into enantiomers of the starting monomer

2-[5-(2,5'-bithienyl)]thianaphthene was synthesized as a racemate by the route described in [18] and subsequently separated into enantiopure antipodes by chiral HPLC, as described in the same reference.

Electrosynthesis and peeling-off of the inherently chiral membranes

The inherently chiral membranes were prepared by electrooligomerization of the BT_2T_4 monomer (racemate or enantiopure) ~0.0025-0.001 M in CH_3CN +0.1 M $TBAPF_6$ (or, in a single case, in CD_3CN + 0.1 M $LiClO_4$) in a glass minicell (working volume ~2 cm^3) including a indium tin oxide ITO (Kintech Company 10 Ω/sq) or in some case fluorine doped tin oxide FTO (Sigma Aldrich 10 Ω/sq) working electrode, a Pt counter electrode and an aqueous saturated calomel electrode SCE as reference electrode; to prevent water and chloride leakage in the working electrode compartment, the SCE was inserted in a glass compartment filled with monomer-free working solution and ending with a porous frit. The membrane preparation was carried out by repeated potential cycling around the BT_2T_4 monomer first oxidation peak at 0.05 V/s scan rate, using an Autolab PGSTAT facility operated by dedicated GPES software. Starting with enantiopure (*R*)-(−)-BT_2T_4 or (*S*)-(−)-BT_2T_4 solutions the monomer configuration was retained, resulting in oligo-(*R*)-(−)-BT_2T_4 films or oligo-(*S*)-(−)-BT_2T_4. Oligo-BT_2T_4 racemate films were also prepared from monomer racemate solutions, both for comparison's sake and to carry out preliminary tests avoiding use of the more precious enantiopure monomers. Transferring the thus modified ITO electrode into deionized water, the thin film could be detached, forming a self-supported membrane, which could be managed using a glass pipette.

SEM

Scanning Electron Microscopy (SEM) observations were carried out using a Leo 1430 SEM (Zeiss, Oberkochen, Germany).

TEM

Transmission Electronic Microscopy (TEM) images were obtained by a Zeiss EFTEM LEO 912AB (120 kV) microscope. To obtain average characteristics many different sample areas were analysed. Thin films were grown on Ni TEM grids as such by 4 electrodeposition cycles.

AFM imaging

AFM imaging was performed in air using a Nanoscope Multimode IIId system (Bruker, Santa Barbara, CA, USA) operating in tapping-mode. AFM images were collected using the RMS amplitude of the cantilever as the feedback signal for the vertical sample position. The RMS free amplitude of the cantilever was approximately 15 nm and the relative set-point above 95% of the free amplitude. Rectangular silicon probes with nominal spring constant around 2.5 N/m (NT-MDT, Russia) and cantilever length of 120 µm were used. The cantilever resonance frequency was about 130 kHz. For AFM experiments, the above ultra-flat ITO electrode (RMS roughness < 1 nm on 1x1 $µm^2$ areas as measured by AFM), on which the oligomeric membranes were deposited through electrochemical oligomerization, was glued to a metal disk that was magnetically fixed to the AFM sample holder. Images were recorded at ~1 Hz line rate and a resolution of 512x512 pixels per image was chosen. AFM images were subject to a line-by-line subtraction of linear background to eliminate sample tilt from the images and correct for step-wise changes between individual scan lines.

TGA+DSC

TGA was performed with a single linear 5 °C/min heating ramp from 30°C to 600 °C, under N2 flux (50 cm3/min), by a combined TGA/DSC 3 + STARe system from Mettler-Toledo®, in standard alumina crucibles (No. 00024123, 70 mm3).

BET surface area and Porosity Distribution

The Brunauer-Emmett-Teller (BET) specific surface area was obtained from N_2 adsorption/desorption isotherms at 77 K using a Micromeritics Tristar II apparatus (Tristar II 3020). Measurements were performed many times to assess isotherms reproducibility and accuracy. Surface area was calculated from nitrogen isotherms by B.E.T., using the instrumental software (Version 1.03). Prior to measuring, sample membranes were heat-treated at 90 °C for 8 h 30 min under a N_2 flow to remove adsorbed foreign species.

IR spectroscopy

FTIR measurements were performed in transmission mode by a Jasco spectrometer mod. FT/IR-4100. on (*i*) the BT_2T_4 monomer (*ii*); a sample of electrodeposited oligo-BT_2T_4 film; (*iii*) a sample of closed BT_2T_4 dimers; (*iv*) a sample of closed BT_2T_4 trimers; (*v*) a sample of closed BT_2T_4 tetramers. Samples (*iii*), (*iv*) and (*v*), representative of several film components (as confirmed by HR LDI) were studied for comparison, being available as previously obtained along an organic route [27] The film sample was electrodeposited from the BT_2T_4 in deuterated acetonitrile (Aldrich) + 0.1 M $LiClO_4$ (Aldrich) (a medium affording to minimize aliphatic C-H signals) followed by stability cycles in the monomer-free solution (to eliminate monomer traces). Since this protocol is slightly different from the one used to obtain the membranes assembled in the ISE body, we checked by HR LDI that both protocols resulted in a similar mixture of open and closed oligomers. The ITO covered with the film was placed in an oven at 120°C for one day, then the film was scraped off the support and collected on a watch glass.
Samples (*i*)-(*iv*) were ground and analyzed as KBr pellets. For sample (*v*), available in traces, a sequence of drops of a concentrated dichloromethane solution were placed and let to evaporate on a KBr pellet followed by oven heating to ensure complete solvent elimination.
All the spectra were recorded in the spectral range between 4000 and 400 cm^{-1} with a resolution of 4 cm^{-1} and obtained as result of 256 accumulations.

Chiroptical spectroscopy

ECD spectra for (*R*)- or (*S*)-enantiopure BT_2T_4 films on ITO and FTO, both as such and as detached membranes have been recorded with a Jasco J815SE instrument. All measurements were performed at 200 nm/min scanning speed, 2 nm SBW. Both for film deposited on the working electrode and for detached films, the experiment has been repeated changing the probe orientation and/or side: the recorded signals give in all cases nearly overlapping ECD features.

LDI

High-resolution LDI spectra have been obtained by a MALDI Tof-Tof Autoflex III Spectrometer at UNITECH COSPECT.

Potentiometric membrane tests in classical ISE-like setup

Sensing membrane electrode The membranes were implemented in a commercial Electrode body for ISE with Lemo connector for mounting of ion-selective membranes, with coaxial cable and connector (Fluka, now corresponding to Sigma Aldrich/Merck 45137). Such ISE body includes an Ag|AgCl electrode, acting as ion/electron transductor through the Nernstian half-reaction $AgCl + e^- \rightarrow Ag + Cl^-$ with electrode potential $E = E^\circ_{AgCl} - k\log a_{Cl}$. It also acts as internal fixed potential reference electrode, a fixed a_{Cl} being provided by the internal solution, based on a chloride binary electrolyte, *i.e.*, according to the experiment, 0.01 *m* KCl, 0.01 *m* $CaCl_2$; 0.01 M HCl and 0.01 M L-tyrosine hydrochloride.

External reference electrode An aqueous saturated calomel electrode (SCE) was employed as the external reference, its saturated KCl solution both ensuring a fixed potential and acting as salt bridge minimizing the liquid junction potential forming on its porous frit between internal and external solution.

Potentiometric tests. The above sensing and reference electrodes were assembled in a potentiometric cell setup and reversible cell potential differences were determined by an AMEL 338 mVmeter with high input impedance (~10^{13} Ω) in solutions of increasing concentrations of different binary chloride electrolytes accounting for various transference number differences between cation and anion, including KCl, $CaCl_2$, HCl, as well as L-tyrosine hydrochloride, featuring a larger, chiral cation suitable for chiral experiments. In the $CaCl_2$ case the test was repeated once with a thinner membrane (prepared with 72 electrooligomerization cycles) and twice with a thicker one (108 cycles) with good reproducibility in the potentiometric response.

Ion activities were calculated from ion concentrations using mean activity coefficients from [42] (KCl, HCl) amd from [43] ($CaCl_2$) and applying the Debye-Hückel convention for estimating single ion activity coefficients from mean electrolyte ones. In the HCl case molar concentrations were converted to molal ones using HCl solution density data from [44].

Acknowledgements

Financial support of Fondazione Cariplo and Regione Lombardia (2016-0923 RST−Avviso congiunto FC-RL Sottomisura B) rafforzamento (Enhancing VINCE (Versatile INherently Chiral Electrochemistry)) is gratefully acknowledged. Mariangela Longhi gratefully acknowledges financial support from Fondo per il Finanziamento delle Attività Base di Ricerca-FFABR.

The Authors acknowledge Dr. Elsa Quartapelle Procopio for organic synthesis and separation of cyclic oligomers used as references [27]; Dr. Alessio Orbelli Biroli for profilometry measurements and Claudia Malacrida for voltammetry enantiodiscrimination tests here mentioned (manuscript in preparation [30]); Prof. Francesco Sannicolò and Prof. Sergio Abbate for fruitful discussions, the latter especially concerning the chiroptical study. The Authors also acknowledge: TGA-DSC Mettler facilities available at SmartMatLab at Department of Chemistry, Università degli Studi di Milano, operated by Dr. Serena Cappelli; SEM facilities at Unitech (Università degli Studi di Milano), operated by Dr. Nadia Santo; and MALDI facilities at UNITECH COSPECT, operated by Dr. Marco Pappini.

Keywords: self-standing electroactive chiral membranes • inherent chirality • (*S*)- and (*R*)- enantiopure membranes • closed vs open chiral thiophene-based oligomers • preliminary tests in ISE-like potentiometric setups

[1] R. Xie, L.-Y-Chu, J-G.Deng, *Chem. Soc. Rev.* **2008**, 37, 1243-1263, *and references therein cited.*
[2] A. Higuchi, M. Tamai, Y.-A. Ko, Y.-I. Tagawa, Y.-H. Wu, B. N. Freeman, J.-T. Bing, Y. Chang, Q.-D. Ling, *Polym. Rev.* **2010**, 50, 113-143.
[3] M. Trojanowicz, M. Kaniewska, *Electroanal.* **2009**, 21, 229-238.
[4] R.-I. Stefan-van Staden, *Anal. Meth.* **2010**, 2, 37-40.
[5] A.-I. Stoica, C. Viñas, F. Teixidor, *Chem. Comm.* **2009**, 4988-4990.
[6] L. Xu, J. Hou, Y. Yang, B. Li, S. Chen, *Anal. Meth.* **2012**, 4, 807-811.
[7] Y. Zhou, B. Yu, K. Levon, *Chem. Mater.* **2003**, 15, 2774-2779.
[8] S. Kang, I. Cha, J.G. Han, C. Song, *Mater. Express*, **2013**, 3, 119-126.
[9] J. Hu, A. Stein, P. Bühlmann, *Trends in Analytical Chemistry,* **2016**, 76, 102-114.
[10] M. Cuartero, G.A. Crespo, *Curr. Opin. Electrochem.* **2018**, 10, 98-106.
[11] G. Radecki, H. Radecka, **2013**, Intech open access peer-reviewed chapter, DOI: 10.5772/52803
[12] R.-I. Stefan-van Staden, J. F. Van Staden, *J. Electrochem. Soc.* **2013**, 160, B196-B200.
[13] M. Shamsipur, A.A.M. Beigi, M. Teymouri, S. Rasoolipour, Z. Asfari, *Anal. Chem.* **2009**, 81, 6789-6796.
[14] R. Liang, L. Chen, W. Qin, *Scient. Reports* **2015**, 5, 12462 (9 pages)
[15] H. Zhang, R. Yao, N. Wang, R. Liang, W. Qin, *Anal. Chem.* **2018**, 90, 657-662.
[16] S. Arnaboldi, M. Magni, P. Mussini, *Curr. Opin. Electrochem.* **2018**, 8, 60-72.
[17] S. Arnaboldi, S. Grecchi, M. Magni, P. R. Mussini, *Curr. Opin. Electrochem.* **2018**, 7, 188-199.
[18] F. Sannicolò, S. Arnaboldi, T. Benincori, V. Bonometti, R. Cirilli, L. Dunsch, W. Kutner, G. Longhi, P.R. Mussini, M. Panigati, M. Pierini, S. Rizzo, *Angew. Chem. Int. Ed.* **2014**, 53, 2623-2627
[19] S. Arnaboldi, T. Benincori, R. Cirilli, W. Kutner, M. Magni, P.R. Mussini, K. Noworyta, F. Sannicolò, *Chem. Science*, **2015**, 6, 1706-1711.
[20] S. Arnaboldi, T. Benincori, R. Cirilli, S. Grecchi, L. Santagostini, F. Sannicolò, P. R. Mussini, *Anal. Bioanal. Chem.* **2016**, 408, 7243–7254
[21] F. Sannicolò, P. R. Mussini, T. Benincori, R. Martinazzo, S. Arnaboldi, G. Appoloni, M. Panigati, E. Quartapelle Procopio, V. Marino, R. Cirilli, S. Casolo, W. Kutner, K. Noworyta, A. Pietrzyk-Le, Z. Iskierko, K. Bartold, *Chem. Eur. J.* **2016**, 22, 10839 – 10847
[22] S. Arnaboldi, T. Benincori, A. Penoni, L. Vaghi, R. Cirilli, S. Abbate, G. Longhi, G. Mazzeo, S. Grecchi, M. Panigati, P. R. Mussini, *Chem. Sci.* **2019**, 10, 2708-2717
[23] S. Arnaboldi, S. Cauteruccio, S. Grecchi, T. Benincori, M. Marcaccio, A. Orbelli Biroli, G. Longhi, E. Licandro, P. R. Mussini, *Chem. Sci.*, **2019**, 10, 1539-1548.
[24] F. Sannicolò, S. Rizzo, T. Benincori, W. Kutner, K. Noworyta, J. W. Sobczak, V. Bonometti, L. Falciola, P. R. Mussini, M. Pierini, *Electrochim. Acta*, **2010**, 55, 8352-8364.
[25] G. Longhi, S. Abbate, G. Mazzeo, E. Castiglioni, P. Mussini, T Benincori, R. Martinazzo, F. Sannicolo, *J. Phys. Chem. C* **2014**, 118, 16019-16027.
[26] T. Benincori, S. Gamez-Valenzuela, M. Goll, K. Bruchlos, C. Malacrida, S. Arnaboldi, P. R. Mussini, M. Panigati, J. T. Lopez Navarrete, M. C.Ruiz Delgado, G. Appoloni, S. Ludwigs, *Electrochim. Acta* **2018**, 284, 513-525.
[27] F. Sannicolò, P.R. Mussini, T. Benincori, R. Cirilli, S. Abbate, S. Arnaboldi, S. Casolo, E. Castiglioni, G. Longhi, R. Martinazzo, M. Panigati, M. Pappini, E.Quartapelle Procopio, S. Rizzo, *Chem. Eur. J.* **2014**, 20, 15298-15302.

[28] E. Quartapelle, T. Benincori, G. Appoloni, P.R. Mussini, S. Arnaboldi, C. Carbonera, R. Cirilli, A. Cominetti, L. Longo, R. Martinazzo, M. Panigati, R. Po, *New J. Chem.* **2017**, 41, 10009-10019.

[29] J. Heinze, B. A. Frontana-Uribe, S. Ludwigs, *Chem. Rev.* **2010**, 110, 4724-4771.

[30] Manuscript in preparation, to be submitted to *Electrochim. Acta*.

[31] E. Castiglioni, S. Abbate, G. Longhi, R. Gangemi, *Chirality* **2007**, 19, 941-946.

[32] E. Castiglioni, P. Biscarini, S. Abbate, *Chirality* **2009**, 21, E28-E36.

[33] G. Louarn, J.P. Buisson, S. Lefrant, D. Fichou, *J. Phys. Chem.* **1995**, 99, 11399-11404.

[34] M. Kofranek, T. Kovář, H. Lischka, A. Karpfen, *J. Mol. Struct. THEOCHEM* **1992**, 259, 181-198.

[35] G. Horowitz, B. Bachet, A. Yassar, P. lang, F. Demanze, J.-L. Fave, F. Garnier, *Chem. Mater.* **1995**, 7, 1337-1341.

[36] F. Martinez, R. Voelkel, D. Naegele, H. Naarmann, Mol. *Cryst. Liq. Cryst.* **1989**, 167, 227-232.

[37] V. Hernández, J. Casado, F. J. Ramírez, G. Zotti, S. Hotta, J.T. López Navarrete, *J. Chem. Phys.* **1996**, 104, 9271-9282.

[38] T. Benincori, G. Appoloni, P. R. Mussini, S. Arnaboldi, R. Cirilli, E. Quartapelle Procopio, M. Panigati, S. Abbate, G. Mazzeo, G. Longhi, *Chem. Eur. J.* **2018**, 24, 11082-11093

[39] E. Bakker, P. Buhlmann, E. Pretsch, *Chem. Rev.*, **1997**, 97, 3083-3132

[40] P. Buhlmann, E. Pretsch, E. Bakker, *Chem. Rev.*, **1998**, 98, 1593-1687

[41] E. Zdrachek, E. Bakker, *Anal. Chem.*, **2019**, 91, 2-26

[42] W.J. Hamer, Y.-C. Wu*, J. Phys. Chem. Ref. Data*, **1972**, 1,1047-1099

[43] R.N. Goldberg, *J. Phys. Chem. Ref. Data*, **1981**, 10, 671-764.

[44] S. L. Clegg, A. S. Wexler, *J. Phys. Chem. A*, **2011**, 115, 3393-3460

Entry for the Table of Contents (Please choose one layout)

ARTICLE

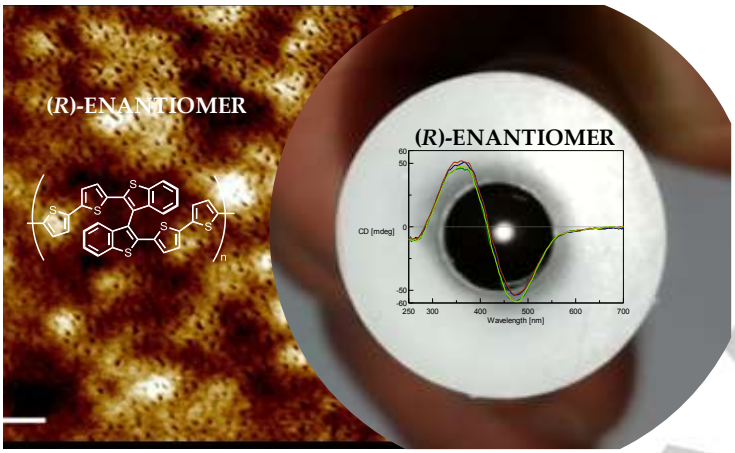

*Author(s), Corresponding Author(s)**

Page No. – Page No.

Title

Electrosynthesis of self-standing chiral electroactive membranes, consisting of "inherently chiral" electroactive open and closed oligomers, with high chiroptical manifestations, characterized and preliminarily tested in an ISE-like potentiometric setup.